Ecological Indicators 171 (2025) 113076

Contents lists available at ScienceDirect

Ecological Indicators

journal homepage: www.elsevier.com/locate/ecolind

Original Articles

An ecosystem resilience index that integrates measures of vegetation function, structure, and composition

Marie Johnson [a,*], Ashley Ballantyne [a], Jon Graham [b], Zachary Holden [c], Zachary Hoylman [d,e], Kelsey Jensco [d,e], David Ketchum [e], John Kimball [f], Jessica Mitchell [g]

[a] Department of Ecosystem and Conservation Sciences, W.A. Franke College of Forestry and Conservation, University of Montana, Missoula, Montana, USA
[b] Department of Mathematical Sciences, University of Montana, Missoula, Montana, USA
[c] U.S. Forest Service, Missoula, Montana, USA
[d] Department of Forest Management, W.A. Franke College of Forestry and Conservation, University of Montana, Missoula, Montana, USA
[e] Montana Climate Office, W.A. Franke College of Forestry and Conservation, University of Montana, Missoula, Montana, USA
[f] Numerical Terradynamic Simulation Group, W.A. Franke College of Forestry and Conservation, University of Montana, USA
[g] Spatial Analysis Lab, University of Montana, Missoula, Montana, USA

ARTICLE INFO

Keywords:
Ecosystem resilience index
Ecological resilience
Wildfire
Ecosystem function
Ecosystem structure
Ecosystem composition
Remote sensing

ABSTRACT

As ecosystem disturbances increase due to human induced global change, accurately quantifying ecosystem resilience has never been more critical. This study introduces a spatially explicit Ecosystem Resilience Index (ERI), that integrates vegetation function, structure, and composition recovery metrics. We provide proof-of-concept for this index by applying it to a wildfire in northwestern Montana by leveraging novel and existing remote sensing datasets to evaluate ecosystem resilience and environmental drivers. First, we independently assessed each metric of ecosystem recovery, and examined how each recovery metric was influenced by abiotic and biotic environmental drivers. We found that ecosystem structure, as estimated by canopy height, showed the highest level of recovery (62 %), followed by composition as measured by relative vegetation abundance (60 %) and function as measured by primary productivity (35 %) over 17 years. Our study revealed that each ecosystem recovery metric is influenced by distinct environmental drivers. Specifically, structural recovery was strongly predicted by distance to seed source, and solar radiation. Compositional recovery was predominantly driven by solar radiation and available soil water capacity. Lastly, burn severity and the terrain ruggedness index were the primary drivers of functional recovery. Finally, we synthesized each ecosystem recovery metric into our ERI, revealing that the overall resilience in our study domain was 54 %. Our estimated ERI rate of 3 %/yr indicates that this forested ecosystem located within the Western Canadian Rockies Ecoregion remains resilient compared to its historical fire return interval of 120 years would yield a 100 % ERI. ERI was driven by solar radiation, distance to seed source, and burn severity. Our findings illustrate that different ecosystem recovery metrics may not provide similar estimates of ecosystem resilience and that recovery metrics may be sensitive to different environmental drivers. Thus an index that incorporates multiple recovery metrics provides a more comprehensive understanding of ecosystem resilience.

1. Introduction

Integrated measures of ecological resilience are critical to our understanding of how ecosystems respond to disturbance under global change. Ecosystem function, structure, and composition of forests are changing in response to multiple global stressors (Coop et al. 2020; Seidl and Turner 2022; Hagmann et al. 2021). Forests currently sequester about one quarter of anthropogenic CO_2 emissions and have the potential to contribute to nature-based climate solutions (Bonan 2008; Pan et al. 2011). However, projected wildfire intensification threatens the climate-regulating services forests provide (Z. Liu, Ballantyne, and Cooper 2019).

* Corresponding author.
E-mail addresses: marie3.johnson@umconnect.umt.edu (M. Johnson), ashley.ballantyne@mso.umt.edu (A. Ballantyne), jgraham@mso.umt.edu (J. Graham), zachary.holden@usda.gov (Z. Holden), zachary.hoylman@mso.umt.edu (Z. Hoylman), kelsey.jencso@mso.umt.edu (K. Jensco), david2.ketchum@umconnect.umt.edu (D. Ketchum), john.kimball@mso.umt.edu (J. Kimball), jessica.mitchell@mso.umt.edu (J. Mitchell).

https://doi.org/10.1016/j.ecolind.2025.113076
Received 13 August 2024; Received in revised form 20 December 2024; Accepted 2 January 2025
Available online 18 February 2025

Although forest ecosystems have been shaped by fire for millions of years (Bowman et al. 2009), evidence suggests that accelerating climate change is leading to rapid changes in wildfire regimes (Keyser and Leroy Westerling 2017). Wildfires in certain regions are occurring with greater frequency, severity, and scale than has been observed in the 20th century (Ward et al. 2012; Higuera, Shuman, and Wolf 2021). These impacts are being seen widely in the western US, where annual burned area has nearly doubled in the past 30 years due to anthropogenically driven increases in fuel aridity and to a lesser extent fuel abundance due to historical fire suppression (Abatzoglou and Williams 2016). These changes underscore the need to understand and quantify ecosystem resilience to disturbance, particularly wildfire. While we have a theoretical understanding of ecological resilience, integrated approaches to quantify resilience at both landscape and regional scales remain limited (Standish et al. 2014; Albrich et al. 2020).

1.1. Ecosystem resilience

The precise definition of ecological resilience is still actively debated (B. H. Walker 2020). Numerous theoretical frameworks have been suggested to classify resilience (Holling 1973; Gunderson 2000; Scheffer et al. 2001), but often lack quantifiable measures applicable across diverse ecosystems. A comprehensive definition of resilience emphasizes the capacity of an ecosystem to return to its pre-disturbance state, regaining ecosystem function, structure, and composition (Thompson et al. 2009).

Efforts to operationalize resilience have advanced through frameworks emphasizing spatial and temporal dimensions, recognizing the role of scale, location, and connectivity in ecosystem responses to disturbance (Allen et al. 2016; Chambers, Allen, and Cushman 2019). Despite these theoretical advancements, many existing approaches focus on singular dimensions of resilience. For example, resilience indices have been developed to measure structural recovery metrics (Bryant et al. 2019; Ibáñez et al. 2019), species-specific assessments (Keane et al. 2018), and bioclimatic indices (Ferrier et al. 2020). While useful, these approaches do not fully capture the complexity of ecosystem recovery processes. A comprehensive resilience framework must integrate function, structure, and composition – three critical attributes that can be quantitatively measured to determine ecosystem resilience to disturbance.

Remote sensing technologies offer an opportunity to address the quantification of resilience. Unlike field-based studies, which are often constrained by scale, remote sensing enables the consistent measurement of ecosystem attributes across large spatial extents. For example, Landsat imagery provides nearly four decades of estimates of primary productivity (function), while advances in full-waveform Lidar, such as the Global Ecosystem Dynamics Investigation (GEDI) mission, enable detailed mapping of canopy height (structure) at high spatial resolutions (R. Dubayah et al. 2020). These technologies allow researchers to monitor spatial and temporal patterns of resilience, from local landscapes to regional and global scales (Hwang et al. 2023). Integrating remotely sensed data into a resilience index enhances our understanding and makes resilience estimation broadly applicable.

In this study, we build upon these theoretical and operational frameworks to define resilience as the capacity of ecosystems to recover following disturbance. Our approach does not require a return to exact pre-disturbance conditions but instead evaluates the recovery of function, structure, and composition on a continuum both independently and collectively. Using an integrated index, we seek to quantify resilience over time and across spatial scales, offering a flexible and operationally useful tool for assessing ecosystem responses to wildfire and other disturbances.

1.2. Ecosystem recovery metrics of resilience

Extensive research has been performed utilizing various remotely-sensed metrics to study functional recovery from wildfires and the environmental variables influencing it; however, regional disagreements in drivers and recovery rates persist. Researchers have quantified postfire functional recovery at regional scales from satellite observations using the Normalized Difference Vegetation Index (NDVI) (Goetz, Fiske, and Bunn 2006; Spasojevic et al. 2016), the Enhanced Vegetation Index (EVI) (Li et al. 2018), Net Primary Production (NPP) (Sparks et al. 2018; Hicke et al. 2003) and Land Surface Temperature (Z. Liu, Ballantyne, and Cooper 2019). These studies show rapid recovery of function in grasslands (2–5 years) and longer recovery rates in forested ecosystems (5–16 years). Forest ecosystem recovery rates varied mostly depending on region and biome. For example, boreal forest recovery rates varied from 5-16 years, whereas temperate forests showed less variability and shorter recovery times between 5–10 years. Despite the abundance of studies on postfire functional recovery, there are regional disagreements in terms of the environmental drivers. Field studies suggest site water balance (Reed et al. 1999), elevation, and soil class (Turner et al. 2004) influence recovery rates. In boreal Alaska, fire chronosequences showed time since fire and forest type (mesic vs. xeric) influenced recovery more than fire history, with linear recovery in wetter sites and logarithmic in drier sites (Mack et al. 2008). Burn severity has also been cited as a primary factor influencing functional recovery (Bright et al. 2019). For example, reduced recovery of NDVI in forests of British Columbia was observed on south facing slope aspects and in areas of high burn severity (Ireland and Petropoulos 2015). Despite these insights, regional discrepancies underscore the need for more research to understand environmental drivers across ecosystems.

Quantifying the recovery of ecosystem structure and characterizing environmental drivers is crucial for examining ecosystem resilience, yet research involving spatially and temporally continuous structural metrics across various ecoregions remains limited. Tracking ecosystem structural recovery following wildfire can help identify stand development pathways in forests (Berkey et al. 2021), and may provide early warning signs of ecosystem transformations (Coop et al. 2020). Although structural recovery has been loosely defined in the literature (Bartels et al. 2016), remote sensing studies have used canopy height and biomass as measures of recovery (Frolking et al. 2009). A *meta*-analysis on Canadian boreal forests revealed that within 5–10 years, canopy height reached only 50 % and canopy cover only 10 % of prefire conditions (Bartels et al. 2016). In boreal Alaska stands were approximately half as tall as unburned stands 20–25 years postfire, with this outcome being primarily influenced by high burn severity (Bolton, Coops, and Wulder 2015). Forests in California have shown structural shifts toward lower density, smaller trees and an increased prevalence of oak species, in response to fire due to fuels accumulation and increased climate water deficits (McIntyre et al. 2015). Many other factors influencing structural recovery have been identified including distance to seed source (Busby, Moffett, and Holz 2020), pre-disturbance forest density and structural heterogeneity (Bolton, Coops, and Wulder 2015; Koontz et al. 2019; Lydersen and North 2012), fire return intervals (Busby, Moffett, and Holz 2020), postfire microclimate (Wolf et al. 2021), topography, and edaphic characteristics (Bartels et al. 2016; Mansuy, Gauthier, and Robitaille 2012). These are valuable findings, however, significant gaps remain in our understanding of structural recovery over greater spatial and temporal scales.

Although numerous research efforts have been made in attempt to capture the complexities of ecosystem compositional recovery following fire, it remains one of the most challenging metrics to quantify. Considerable effort has been made to measure the recovery of tree species following wildfire through extensive field studies across the western US (Stevens-Rumann and Morgan 2019; Kimberley T. Davis et al. 2023). These studies offer valuable insights into the dynamics of tree species regeneration and the effects of climate and fire severity. However, to gain a more comprehensive understanding of compositional recovery, it is crucial to examine the recovery and roles of understory vegetation, which these studies have highlighted as an important area for further research. Researchers have characterized evergreen and deciduous vegetation regeneration rates postfire in the western US using dual-season NDVI (Vanderhoof et al. 2021). However, additional work is needed to identify vegetation types more precisely by differentiating tree saplings from shrubs, and characterizing grasses following wildfire at regional scales. A study by (J. J. Walker and Soulard 2019), developed a methodology that utilizes coarse resolution MODIS NDVI phenological signals to identify the recovery patterns of dominant vegetation types, including shrublands, conifer-dominated forests, and grasslands, across selected fire sites in Arizona and New Mexico. These studies have identified key environmental factors influencing the recovery of composition, including burn severity, distance to seed source, increased atmospheric moisture demand, and maximum temperature, that influence the recovery or failure of conifer and deciduous trees following wildfire. Although these studies significantly contribute to our understanding of the factors driving tree regeneration, further research is needed to comprehensively track the recovery of vegetation composition following wildfire and its associated environmental drivers.

1.3. Study framework and Objectives

Here we present an integrated approach to estimate ecosystem resilience *(*Fig. 1*)*. We hypothesize that ecosystem function, structure, and composition will recover at different rates following wildfire and be responsive to different abiotic and biotic environmental drivers. Specifically:

1. Ecosystem function (measured by NPP) will recover first, and will be primarily controlled by burn severity and microclimatic drivers affecting plant water availability.
2. Ecosystem structure (measured by canopy height) will recover more slowly, driven primarily by burn severity and secondarily by topography.
3. Ecosystem composition (measured by relative abundance of vegetation functional types) will recover last, primarily driven by burn severity and secondarily by distance to seed source.

Objectives:

1. To quantify the recovery of ecosystem function, structure, and composition, following a severe wildfire using remotely sensed metrics.
2. To develop an integrated Ecosystem Resilience Index (ERI) that combines recovery rates and magnitudes of recovery across function, structure, and composition.
3. To identify the primary environmental drivers (e.g., burn severity, microclimatic variables, topography, and distance to seed source) that influence the recovery of ecosystem attributes and resilience.
4. To demonstrate the effectiveness of the ERI in measuring and comparing resilience across a postfire landscape.

2. Methods

2.1. Study domain

Our study focuses on the Crazy Horse Fire, a severe wildfire that occurred in northwestern Montana on August 10th, 2003 in the Mission Wilderness of northwestern Montana (Fig. 2). This area is located on the traditional and ancestral territory of the Confederated Salish and Kootenai People, and lies within the Western Canadian Rockies Ecoregion which is strongly influenced by moist maritime air masses (Omernik and Griffith 2014). The burned area receives an average of 1500 mm of precipitation annually, with a mean annual temperature of 2.5 °C based on a 30 year average (1991–2020) (PRISM Climate Group 2014). The area is characterized by complex, rugged terrain, and alpine lakes. Elevation within the fire disturbance area ranges from 1,240 m to 2,416 m.

The study area is historically comprised of mixed-coniferous forest, containing douglas-fir (*P. menziesii*), lodgepole pine (*P. contorta*), western larch (*L. occidentalis*), engelmann spruce (*P. engelmannii*), subalpine fir (*A. lasiocarpa*), grand-fir (*A. grandis*), ponderosa pine (*P. ponderosa*), with western red cedar (*T. plicata*) and western hemlock (*T. heterophylla*) growing in valley bottoms and quaking aspen (*P. tremuloides*) in riparian zones. Common understory vegetation in the Mission Wilderness includes deciduous shrubs (*P. malvaceus, P. virginiana, H. discolor, R. woodsii, V. globulare*), the perennial herb Bear Grass (*X. tenax)*, and small Rocky Mountain Maple trees (*A. glabrum*) (Alt et al. 2018). Prior to the fire, 65 % of the vegetation within the burn perimeter was classified as upper elevation tree species (subalpine fir, grand fir and lodgepole pine) (Calkin et al. 2005).

Historically, the study domain experienced a mean fire return interval of approximately 120 +/- 140 (SD) years (Greenberg et al. 2021). According to the National USFS Fire Perimeter database, with the exception of the Crazy Horse Fire, only 6 small fires (19–121 acres) occurred in the Mission Wilderness between 1900 and 2022. The burn overlapped with the Mission Wilderness (45 %), Flathead National Forest (32 %) and Plum Creek timberland (23 %) (Calkin et al. 2005). In order to control for management practices, this analysis was performed only on the Mission Wilderness portion of the fire affected study area *(*Fig. 2*)*.

2.2. Recovery metrics

To provide an integrated framework of ecosystem resilience we selected one recovery metric for each ecosystem attribute (Fig. 1*a*). We allowed for an extended prefire burn period for our analysis of function (NPP) and composition (vegetation functional types) by selecting recovery metrics that exist from 1986 to 2020. To leverage observations of

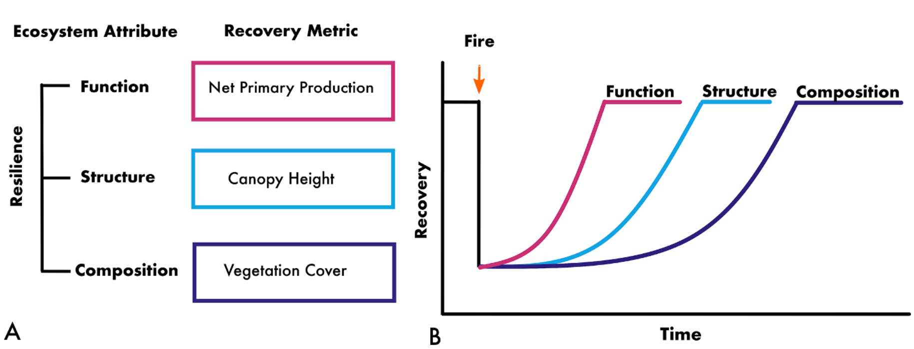

Fig. 1. Conceptual diagram of integrated ecosystem resilience. (a) Ecosystem attributes of resilience (function, structure, and composition) and their corresponding recovery metrics (Net Primary Production, canopy height, and vegetation cover). (b) Idealized recovery of each ecosystem attribute following wildfire.

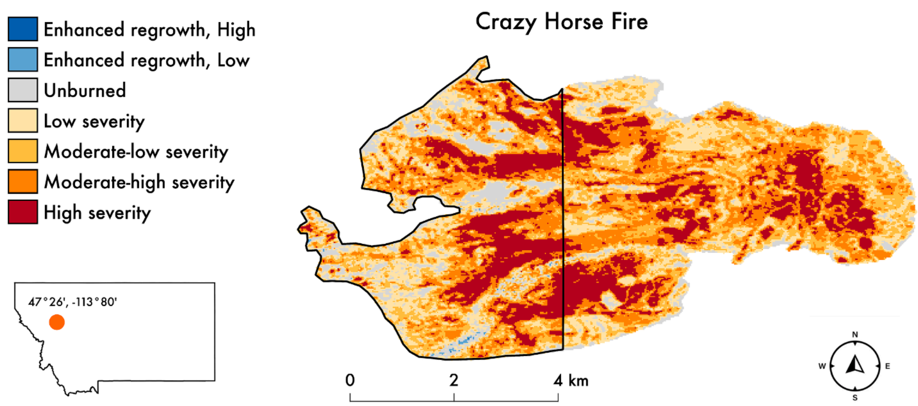

Fig. 2. Burn severity estimated from the differenced Normalized Burn Ratio at the Crazy Horse Wildfire that occurred in August 2003. The map outline represents the Mission Wilderness area over which this study was performed.

structure in the absence of temporally and spatially continuous structural data at high resolutions, we incorporated temporally static data of canopy height from 2020, derived from the Global Ecosystem Dynamics Investigation (GEDI) (R. Dubayah et al. 2020; Lang et al. 2023). We used Google Earth Engine to extract each recovery metric (Gorelick et al. 2017). With this selection of recovery metrics, we estimated functional, structural, and compositional recovery independently across the fire disturbance recovery area and linked them to abiotic and biotic environmental drivers.

2.3. Recovery models

To accurately estimate the recovery of each metric we developed specific models tailored to the properties (i.e. spatio-temporal capacities) of the available data. For our temporally continuous metrics (NPP and fractional cover), we developed a flexible model to account for the temporal variability of ecological data. This model operates on each 30-m pixel within the domain, employing a piecewise function to estimate a pre-fire reference mean and a generalized additive model (GAM; Eq. (1) post-fire for tracking percent recovery over time, with linear predictor of the form:

$$\eta_i = \beta_0 + \beta_1 I(t_i \leq 17) + f(t_i \cdot (1 - I(t_i \leq 17))) \quad (1)$$

using an identity link function, where, η_i is the linear predictor for the i^{th} i observation, β_0 is the intercept term, β_1 is the coefficient for the indicator variable, $I(t_i \leq 17)$, t_i is the year for the i^{th} observation, f is a smooth function of $t_i \bullet (1 - I(t_i \leq 17))$, represented using $k = 10$ basis functions, $I(t_i \leq 17)$ is an indicator function that equals 1 if $t_i \leq 17$ (prefire period) and 0 otherwise (postfire period).

This approach aligns more closely with our conceptual framework (Fig. 1*b*). Using this framework, percent recovery was calculated using a baseline from the minimum postfire value observed between 2003 and 2020 (*Eq. (2)*. Here, RM represents a given recovery metric, and $\hat{Y}$ is our estimate of percent recovery.

$$\hat{Y}_{Percent\ Recovery} = \left(\frac{RM_{2020} - RM_{minimum\ postfire}}{RM_{prefire} - RM_{minimum\ postfire}}\right) \times 100 \quad (2)$$

If a location did not experience significant change (did not exceed the 95 % prefire confidence interval) from the prefire mean to the postfire minimum, it was excluded from further analysis. The minimum postfire value was used because in some cases a recovery metric continued to decline after the year of the fire. Therefore, percent recovery was calculated using the minimum value that occurred from 2003 to 2020, instead of using the value at the year of the fire. Adaptations to the percent recovery model will be specified in the following sections based on the selected dataset.

2.4. Ecosystem functional recovery

To estimate functional recovery following fire, we used high resolution (30 m) remotely sensed Net Primary Production (NPP; $gC\,m^{-2}\,y^{-1}$) from 1986 to 2020 and applied our GAM recovery model. This mean annual NPP product (Robinson et al. 2018), derived from Landsat data and the Moderate Resolution Imaging Spectroradiometer (MODIS) MOD17 algorithm (S. W. Running et al. 2004), provides a robust and scalable measure of ecosystem function by integrating photosynthetic capacity and carbon allocation. NPP has been widely used to assess post-disturbance recovery across ecosystems (Z. H. Hoylman et al. 2021; T. S. Davis et al. 2022) and has successfully captured shifts in vegetation productivity following wildfire (Sparks et al. 2018; Hicke et al. 2003). While NPP does not capture all aspects of ecosystem function, such as nutrient cycling, or belowground processes like soil respiration, it offers a consistent and interpretable metric for quantifying functional recovery across large spatial and temporal scales.

2.5. Ecosystem structural recovery

To estimate the recovery of forest structure following fire we employed a 10 m resolution Sentinel interpolated canopy height product derived from the GEDI dataset for the year 2020 (Lang et al. 2023). These data resolve the 3 m minimum detection limit presented by the raw GEDI waveform dataset (A. Liu, Cheng, and Chen 2021). Canopy height can act as an indicator of ecosystem structure because it reflects changes in vegetation regrowth, biomass accumulation, and can be used to gauge successional stages within a post-disturbance landscape (Hwang et al. 2023). While complimentary data, such as canopy density, layering, and canopy openness, provide insights into structural changes, we used canopy height due to its global availability at high resolution to serve as a robust and interpretable metric for assessing post-disturbance structural recovery. Due to the lack of continuous historical canopy height data, we were unable to consider a prefire baseline period, as we did for the analyses of functional and compositional recovery. Instead, we employed an alternative approach to create a spatially continuous potential canopy height in the absence of a prefire reference.

We used a random forest (RF) model to predict an unburned potential canopy height within the burned area. RF was chosen for its robustness and flexibility, as it can effectively model complex, nonlinear relationships commonly observed in ecological datasets. By combining predictions from multiple decision trees trained on bootstrap samples and introducing randomness in feature selection, RF reduces overfitting and achieves high accuracy. Its ability to handle complex interactions and variability makes it well-suited for predicting canopy height across highly heterogeneous landscapes. Additionally, RF has been shown to outperform traditional imputation and regression methods in terms of accuracy and bias, particularly when applied to forest structural attributes using LiDAR-derived and related remote sensing data (Hudak et al. 2008; Breiman 2001).

To train the RF model, we sampled 40,000 randomly distributed points from the surrounding unburned Mission Wilderness and extracted an array of topographic, climate, and edaphic variables. This dataset allowed the RF to learn spatial patterns and predict potential canopy height at each pixel within the burned area. The Mission Wilderness, a minimally disturbed landscape, was an advantageous choice for training the RF model because it has experienced little to no management. The burned area spanned both wilderness and national forest land; however, we specifically chose to incorporate only the wilderness portion of the burn to avoid introducing potential bias or variability associated with management practices on the national forest land. Such practices could alter vegetation recovery trajectories and affect the comparability of canopy height estimates. According to the National USFS Fire Perimeter database, only six small fires (ranging from 19 to 121 acres) occurred in the Mission Wilderness between 1900 and 2022, with the exception of the Crazy Horse Fire. We calculated percent recovery as the observed canopy height divided by the predicted unburned potential canopy height. For simplicity, we refer to this estimate as percent recovery and describe it as a recovery rate, despite the lack of continuous temporal canopy height data.

2.6. Ecosystem compositional recovery

We selected a recently developed vegetation classification algorithm to estimate the recovery of vegetation fractional cover following fire (Matthew O. Jones et al. 2018; Allred, Bestelmeyer, and Boyd 2021). This product derived fractional cover for six cover classifications: annual forb and grasses (AFG), perennial forb and grasses (PFG), shrubs (SHR), trees (TRE), litter (LTR), and bare ground (BGR). Although this product was originally developed for rangelands, additional training data from forest inventories has been incorporated to successfully detect changes in tree cover over the western US (Morford et al. 2021). To estimate the recovery of composition in the burned area, we used a modified version of the GAM percent recovery model. To estimate the recovery of composition in the burned area, we used a modified version of the GAM percent recovery model. We performed a pixel-wise principal component analysis (PCA) using the six classes of fractional cover incorporating data from 1986 to 2020. We then extracted the scores from the first principal component (PC1) to use in our GAM recovery model and estimated the percent recovery of composition at each pixel in 2020.

2.7. Ecosystem resilience Index

We synthesized the results of the functional, structural and compositional recovery metrics from our study to create a spatially explicit Ecosystem Resilience Index (ERI) at a 30 m spatial resolution. To estimate ecosystem resilience we combined the percent recovery of vegetation function, structure, and composition using an inverse variance weighting approach, which combines estimates with more weight given to estimates that are more precise (i.e., lower variance) (Lee et al. 2016).

$$\widehat{\theta}_{ERI} = \frac{\sum_{i=1}^{n} w_i \widehat{\theta_i}}{\sum_{i=1}^{n} w_i} \tag{3}$$

$$w_i = 1/\sigma_i^2$$

Where $\widehat{\theta}_{ERI}$ is the combined estimate of resilience, $n = 3$ representing each ecosystem attribute (i.e., function, structure, and composition), and $\widehat{\theta}_i$ is the estimate for each ecosystem attribute. w_i is the weight given to each ecosystem attribute, using the inverse variance for each ecosystem attribute.

To estimate consistent recovery rates across metrics and our overall resilience rate, we assumed a linear recovery based on the mean percent recovery in 2020.

2.8. Selection of environmental drivers

We selected a suite of environmental drivers to evaluate their influence on ecosystem recovery metrics and the overall resilience index (Table 1). Abiotic factors included burn severity (differenced Normalized Burn Ratio, dNBR), topographic indices (Topographic Position Index, TPI; Topographic Wetness Index, TWI; Terrain Ruggedness Index, TRI), cold air drainage (CAD), available soil water storage capacity (AWS), and climate variables (annual net solar radiation, SRAD; climate water deficit, CWD). One biotic factor, distance to seed source (DTS), was also included.These variables were chosen for their relevance in explaining recovery patterns and potential for informing management strategies. For example, areas with high AWS could be prioritized for replanting, while specific management plans could target areas with reduced resilience to encourage ecosystem transformation.

Burn severity was assessed using dNBR from the Monitoring Trends in Burn Severity (MTBS) database (Eidenshink et al. 2007) calculated, as the difference in Normalized Burn Ratio one year pre and postfire. Terrain variables (TPI, TWI, TRI) and elevation were derived from the Shuttle Radar Topography Mission elevation dataset (Rabus et al. 2003). TPI measures landscape position, with negative values indicating valleys and positive values indicating ridgetops, which can influence temperature, soil development, and soil moisture availability (De Reu et al. 2013; Parker 1982). TWI estimates water availability based on upslope contributing area and flow width, which is linked to conifer basal area growth rates (Zachary H. Hoylman et al. 2018; Beven and Kirkby 1979). The TRI quantifies topographic complexity, which can influence microclimates and seedling survival, and offer structural niches for terrestrial plant species (Riley, DeGloria, and Elliot 1999; Marsh et al. 2022).

Biophysical variables included CAD, which represents nocturnal cold air pooling that buffers vegetation against heat stress, AWS to represent soil water storage, and SRAD to capture solar energy, corrected for slope and aspect. We also incorporated 30-year averages of CWD to reflect climate related limitations on recovery (Holden et al. 2018). DTS, representing distance to reproductively mature trees (≥3 m height), was extracted from the USFS Topofire Regeneration Mapper (Holden et al. 2022) and known to be a key predictor of forest recovery (Stevens-Rumann and Morgan 2019).

Multicollinearity among variables was tested using a variance inflation factor threshold of 4.0. None of the selected variables exceeded this threshold, ensuring they could be included in the analysis.

2.9. Spatial statistical analysis

We selected a spatial statistical model to examine predictors of recovery because ecological processes and disturbances like wildfires are often found to exhibit spatial autocorrelation (Ver Hoef et al. 2018; Prichard et al. 2020). Spatial autocorrelation (SAC) occurs when observations close in space are more similar than those far apart. The likelihood of Type I errors increases when SAC is present and not explicitly modeled because it violates the assumption of independence between observations (Bivand, Pebesma, and Gomez-Rubio 2013). The incorporation of spatial structure can yield more accurate models by reducing Type I errors that may lead to inaccurate coefficient estimates and corresponding standard errors (Prichard et al. 2020).

To begin, we examined the direction of spatial continuity and distance within which SAC is present and constructed robust variograms using the Cressie-Hawkins estimator (Cressie and Hawkins 1980). We fit isotropic and anisotropic variograms for each recovery metric and the resilience index. Secondly, to identify environmental predictors of

Table 1
Description and native scale of environmental drivers used in the spatial conditional autoregressive model analysis of the recovery of ecosystem attributes and the ecosystem resilience index.

Variable	Units and scale	Description and source	Represents	Source
Annual net solar radiation (SRAD)	W/m2, 30 *m*	Incoming shortwave radiation	Energy	Holden et al. 2018
Available soil water storage capacity (AWS)	mm per m, 30 *m*	Capacity of soil to store water	Soils, Water	Holden et al. 2019
Cold air drainage (CAD)	Degrees C, 30 *m*	Nocturnal pooling of cold, dense air resulting in temperature inversions as elevation decreases toward valley bottoms	Daily temperature gradient	Holden et al. 2020
Climate water deficit (CWD)	mm, 30 *m*	Potential evapotranspiration − actual evapotranspiration	Climate	Holden et al. 2018
differenced Normalized Burn Ratio (dNBR)	Unitless, 30 *m*	The Normalized Burn Ratio one year prior to the fire and one year postfire to describe burn severity	Burn severity	Eidenshink et al. 2007
Distance to seed source (DTS)	m, 30 *m*	Distance from nearest living adult tree	Seed availability	Holden et al. 2022
Topographic position index (TPI)	Unitless, 30 *m*	Relative landscape position	Temperature, moisture	Rabus et al. 2003
Terrain Ruggedness Index (TRI)	Unitless, 30 *m*	The sum of change in elevation in surrounding pixels based on a digital elevation model	Topographic diversity	Rabus et al. 2003
Topographic wetness index (TWI)	Unitless, 30 *m*	Estimates water supply to a specific location using the upper catchment area, flow width, and down slope drainage	Water availability	Rabus et al. 2003

recovery and resilience we used a spatial conditional autoregressive (CAR) model. The CAR model exploits SAC to fit models by incorporating spatial structure in the model's covariance matrix. The CAR model is considered conditional because each variable of the random process at a specific location (pixel) is conditioned on the values in neighboring sites (Ver Hoef et al. 2018):

$$\mathbf{Y} = \mathbf{X}\boldsymbol{\beta} + \rho\mathbf{W}(\mathbf{Y} - \mathbf{X}\boldsymbol{\beta}) + \boldsymbol{\varepsilon}, \quad \text{with} \quad \boldsymbol{\varepsilon} \sim \mathcal{N}(\mathbf{0}, \sigma^2\mathbf{I}) \tag{4}$$

where $\mathbf{Y}$ is the vector of response variables at all locations, $\mathbf{W}$ is a neighborhood weight matrix that specifies neighboring weights for each pixel, ρ is the spatial autocorrelation parameter to estimate the strength of spatial autocorrelation, β is the usual vector of coefficients corresponding to the matrix of explanatory variables $\boldsymbol{X}$, and $\boldsymbol{\varepsilon}$ is assumed to be a multivariate normal error vector. The response variable Y_i at a given site i is dependent on the values of neighboring responses (Y_j); that is, Y_i is regressed on itself through its neighboring values. We implemented the CAR model using coarsened 90 m resolution data due to computational constraints. We selected the spmodel (Dumelle, Higham, and Ver Hoef 2023) package in R and used the spautor function to perform a CAR analysis. Using a first-order neighborhood structure, we set the neighborhood distance to 90 m. We initially fit a null spatial model of percent recovery (and resilience index) with no predictors. To assess improvement in model fit with the addition of spatial structure from a non-spatial linear model we implemented a leave-one-out cross validation technique(Hastie, Tibshirani, and Friedman 2001). In each model of recovery metrics (and the resilience index), the spatial CAR model resulted in a decrease in root mean square error. We then constructed single predictor models to examine and rank each environmental

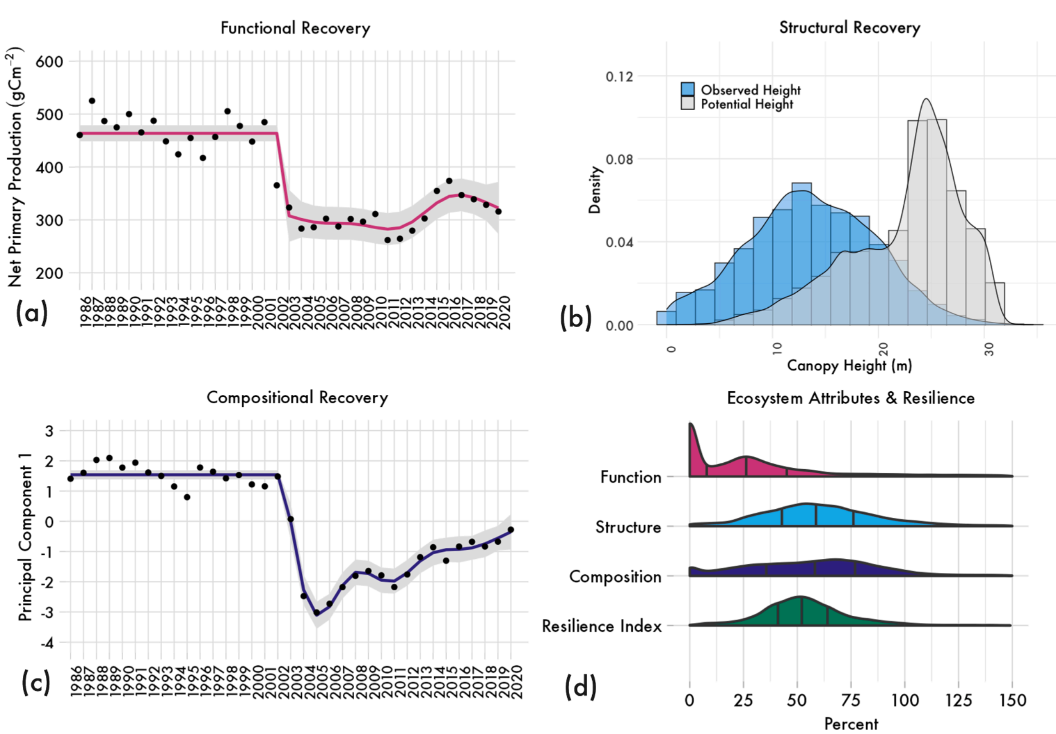

Fig. 3. Recovery of ecosystem attributes following the Crazy Horse Wildfire in 2003. (a) Time series of mean percent recovery of function as measured by Net Primary Production over the study domain, (b) distribution of observed and potential canopy height from which percent recovery of structure was estimated, and (c) time series of mean percent recovery of composition as measured by the first principal component of fractional cover over the study domain. (d) Distributions of each recovery metric and the Ecosystem Resilience Index (ERI).

driver's ability to predict recovery (and the resilience index) as a single predictor variable. We selected models that were shown to be significant and ranked each model by its reduction in Akaike Information Criterion (AIC) (Sakamoto and Akaike 1998) value from the null spatial model.

3. Results

3.1. Ecosystem functional recovery

Overall, the mean estimate of NPP recovery was 35 % (SD +/-49 %) of the preburn condition, with a median value of 23 % (Q1: 0 %, Q3: 43 %) (Fig. 3*d*). We approximate the rate of recovery over 17 years to be 2.0 %/yr, based on the mean recovery value in 2020. The map of NPP recovery (Fig. 4*a*) suggests that recovery is not spatially random, with clearly defined areas of very high or low recovery. This is also reflected in a bimodal distribution of functional recovery (Fig. 3*d*) with modes at ~ 0 % and 25 %. Using a robust variogram estimator, we found the range of spatial autocorrelation to be approximately 1200 m (*Fig. S1a*), with the direction of greatest continuity to be ~ 90 degrees clockwise from North, suggesting a general East-West gradient in functional recovery (*Fig. S1b*).

Among our environmental predictors of functional recovery, physical and terrain characteristics were the most important. Based on the reduction in AIC from the null spatial model, the CAR model revealed that burn severity ($\widehat{\beta}_1$ = -0.049, CI = −0.058, −0.041) was the strongest predictor of reduced NPP recovery following fire. This was followed by terrain ruggedness ($\widehat{\beta}_1$ = 0.75, CI = 0.60, 0.89) and surface radiation ($\widehat{\beta}_1$ = -0.025, CI = −0.031, −0.019). Our analysis also identified DTS ($\widehat{\beta}_1$ = -0.082, CI = −0.10, −0.062), CWD ($\widehat{\beta}_1$ = -0.20, CI = −0.27, −0.12), CAD ($\widehat{\beta}_1$ = -6, CI = −11, −1.3), and AWS ($\widehat{\beta}_1$ = -0.2, CI = −0.32, −0.08) as variables of importance (Fig. 5*a*, Table 2).

3.2. Ecosystem structural recovery

Overall, the mean estimate of canopy height recovery is 62 % (SD +/-75 %), with a median value of 59 % (Q1: 43 %, Q3: 77 %) (Fig. 3*d*). We approximated a linear rate of recovery to be 3.6 %/yr, based on the mean value of recovery in 2020. The canopy height recovery map (Fig. 4*b*) suggests spatial autocorrelation among recovery values. Using a robust variogram estimator, we found the range of spatial autocorrelation to be approximately 4000 m *(Fig. S2a)* with the direction of greatest continuity to be ~ 90 degrees clockwise from North, suggesting a mild East-West gradient similar to NPP (*Fig. S2b*).

Our findings indicate that both abiotic and biotic environmental drivers were important for structural recovery. Based on the reduction in AIC from the null spatial model, the CAR model revealed that solar radiation ($\widehat{\beta}_1$ = -0.037, CI −0.040, −0.034) is the best predictor of

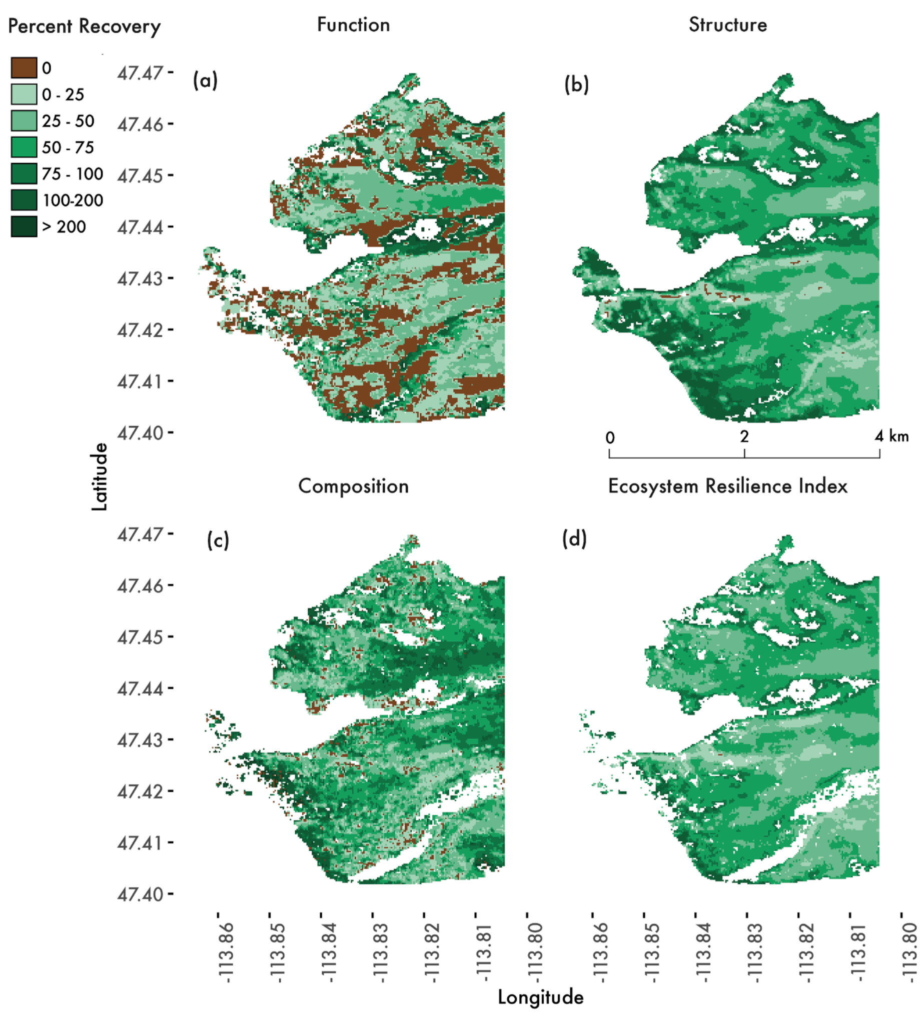

Fig. 4. Maps of (a) percent recovery of function as measured by Net Primary Production, (b) percent recovery of structure as measured by canopy height, (c) percent recovery of composition as measured by the first principal component of fractional cover, and (d) the integrated Ecosystem Resilience Index (ERI).

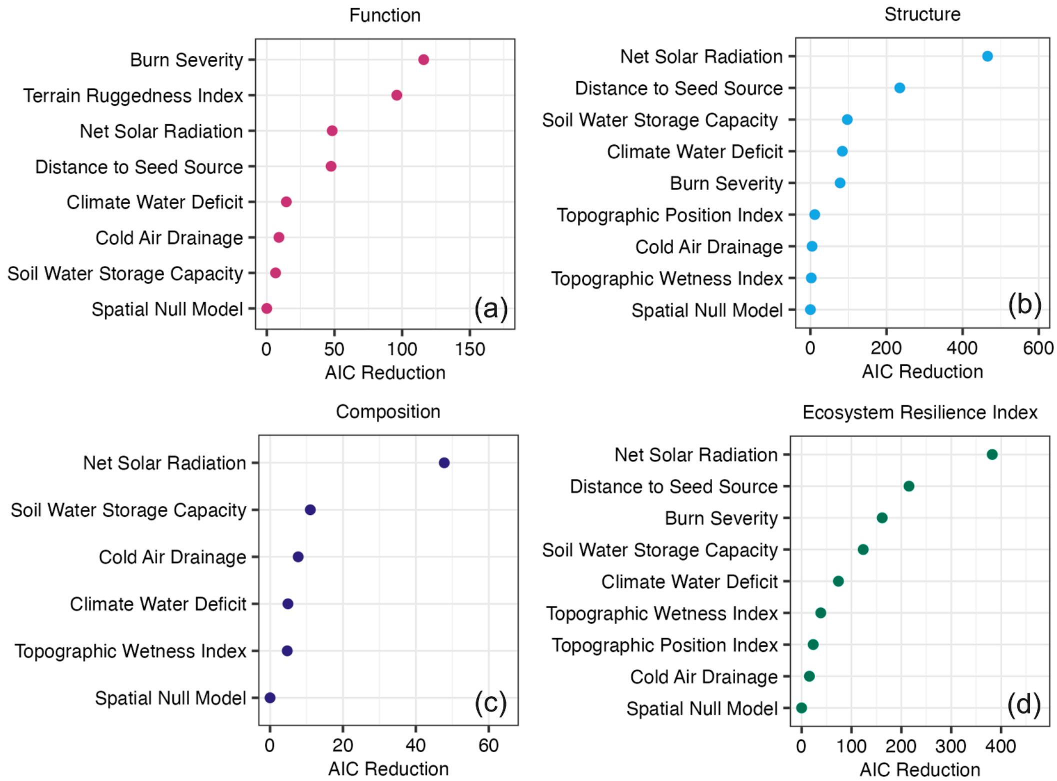

Fig. 5. Akaike information criterion (AIC) reductions from the null spatial conditional autoregressive (CAR) models of the environmental drivers of function (a), structure (b), composition (c), and the Ecosystem Resilience Index (d).

structural recovery, followed by distance to seed source ($\widehat{\beta}_1$ = -0.11, CI = −0.12, −0.09), and available water storage ($\widehat{\beta}_1$ = 0.33, CI = 0.27, 0.29) This was followed by an array of climate-related water variables regulated by topography – CWD ($\widehat{\beta}_1$ = -0.21, CI = −0.26, −0.17), dNBR ($\widehat{\beta}_1$ = 0.021, CI = −0.026, 0.017), TPI ($\widehat{\beta}_1$ = -0.070, CI = −0.10, −0.036), CAD ($\widehat{\beta}_1$ = -5.0, CI = −8.3, −1.7), and TWI ($\widehat{\beta}_1$ = 0.73, CI = 0.20, 1.3) (Fig. 5*b*, Table 2).

3.3. Ecosystem compositional recovery

The mean estimate of compositional recovery as measured by changes in fractional cover of vegetation is 60 % (SD +/-42 %) with a median value of 59 % (Q1: 34 %, Q3: 78 %) (Fig. 3*c*). We approximate a rate of recovery of 3.5 %/yr, based on the mean value of recovery in 2020. Using a robust variogram estimator, the range of spatial autocorrelation was found to be approximately 3700 m (*Fig. S3a*), with the direction of greatest continuity to be ~ 45 degrees clockwise from North, suggesting a Northeast-Southwest gradient different from the other recovery metrics (*Fig. S3b*).

The PCA of vegetation cover data from 1986 to 2020 (averaged over the entire burned area) revealed shifts in compositional recovery patterns before and after the fire. Principal component one (PC1) explained 81 % of the variance in changing vegetation cover when all years were considered *(Fig. S4)*. In the prefire years leading up to 2003, tree cover contributed positively to PC1. In the early postfire years (2004–2009), shrubs, bare ground, annual forbs and grasses, and litter contributed negatively to both PC1 and PC2. In the later postfire years (2010–2020), perennial forbs and grasses primarily drove the variance, contributing negatively to PC1 and positively to PC2. These results suggest a clockwise shift over time from prefire to postfire years in our PCA biplot.

Physical environmental drivers were the primary factors influencing compositional recovery. Similar to factors controlling structural recovery, solar radiation ($\widehat{\beta}_1$ = -0.014, CI = −0.020, −0.010) emerged as the strongest predictor of compositional recovery, albeit with reduced sensitivity compared to structural recovery. This was followed by available soil water storage ($\widehat{\beta}_1$ = 0.21, CI = 0.11, 0.31), CAD ($\widehat{\beta}_1$ = 5.1, CI = 0.45, 9.7), CWD ($\widehat{\beta}_1$ = -0.11, CI = −0.18, −0.04), and TWI ($\widehat{\beta}_1$ = 0.95, CI = −0.07, 1.8) (Fig. 5c, Table 2).

3.4. Ecosystem resilience Index (ERI)

Overall, the mean estimate of ERI is 54 % (SD: +/-21 %) with a median value of 52 % (Q1: 41 %, Q3: 64 %) (Fig. 3*d*). We approximate a resilience rate of 3.2 %/yr, based on the mean value of recovery in 2020. Using a robust variogram estimator, the range of spatial autocorrelation was found to be approximately 2800 m (*Fig. S5a*), with the direction of greatest continuity to be ~ 90 degrees clockwise from North, suggesting a dominant East-West gradient (*Fig. S5b*).

Our findings suggest that integrated resilience is driven by both physical and biological factors. Similar to compositional and structural recovery, solar radiation ($\widehat{\beta}_1$ = -0.026, CI = −0.028, −0.023) was the primary environmental driver of resilience. This was followed by distance to seed source ($\widehat{\beta}_1$ = -0.069, CI = −0.078, −0.060), and burn severity ($\widehat{\beta}_1$ = -0.022, CI = −0.025, 0.018) and a range of climate-related water variables – AWS ($\widehat{\beta}_1$ = 0.26, CI = 0.21, 0.30), CWD ($\widehat{\beta}_1$ = -0.14, CI = −0.17, −0.11), TWI ($\widehat{\beta}_1$ = 1.2, CI = 0.86, 1.6), TPI ($\widehat{\beta}_1$ = -0.080, CI = −0.11, −0.051), and CAD ($\widehat{\beta}_1$ = -4.6, CI = −6.9, −2.3) (Fig. 5*d*, Table 2).

Table 2
Estimates, confidence intervals, p-values and AIC values from the spatial conditional autoregressive models of environmental drivers for each ecosystem attribute and the ecosystem resilience index.

Function						
Model	β_0	95% CI	β_1	95% CI	p-value	AIC
Burn Severity (dNBR)	56	50, 62	−0.05	−0.06, −0.04	<0.001	37,352
Terrain Ruggedness Index (TRI)	16	9.8, 22	0.75	0.60, 0.89	<0.001	37,372
Annual Net Solar Radiation (SRAD)	126	102, 151	−0.03	−0.03, −0.02	<0.001	37,420
Distance to Seed Source (DTS)	49	43, 55	−0.08	−0.10, −0.06	<0.001	37,421
Climate Water Deficit (CWD)	85	63, 107	−0.20	−0.27, −0.12	<0.001	37,454
Cold Air Drainage (CAD)	18	4.6, 31	−6.00	−11, −1.3	0.013	37,459
Available Soil Water Storage Capacity (AWS)	56	41, 70	−0.20	−0.32, −0.08	0.001	37,462
Topographic Wetness Index (TWI)	35	26, 44	−0.35	−1.4, 0.73	0.5	37,467
Spatial Null Model	33	27, 39			<0.001	37,468
Topographic Position Index (TPI)	33	27, 39	−0.08	−0.13, −0.02	0.007	37,471

Structure						
Model	β_0	95% CI	β_1	95% CI	p-value	AIC
Annual Net Solar Radiation (SRAD)	203	185, 221	−0.04	−0.04, −0.03	<0.001	32,942
Distance to Seed Source (DTS)	83	71, 95	−0.11	−0.12, −0.09	<0.001	33,173
Available Soil Water Storage Capacity (AWS)	24	8.5, 40	0.33	0.27, 0.39	<0.001	33,311
Climate Water Deficit (CWD)	118	104, 132	−0.21	−0.26, −0.17	<0.001	33,324
Burn Severity (dNBR)	73	61, 86	−0.02	−0.03, −0.02	<0.001	33,330
Topographic Position Index (TPI)	62	52, 73	−0.07	−0.10, −0.04	<0.001	33,396
Cold Air Drainage (CAD)	49	37, 62	−4.97	−8.3, −1.7	0.003	33,403
Topographic Wetness Index (TWI)	59	50, 68	0.73	0.20, 1.3	0.007	33,405
Spatial Null Model	62	53, 71			<0.001	33,408
Terrain Ruggedness Index (TRI)	59	51, 68	0.12	0.04, 0.19	0.003	33,410

Composition						
Model	β_0	95% CI	β_1	95% CI	p-value	AIC
Annual Net Solar Radiation (SRAD)	113	90, 136	−0.01	−0.02, −0.01	<0.001	33,895
Available Soil Water Storage Capacity (AWS)	42	28, 56	0.21	0.11, 0.31	<0.001	33,932
Cold Air Drainage (CAD)	77	64, 90	5.06	0.45, 9.67	0.032	33,936
Climate Water Deficit (CWD)	95	75, 114	−0.11	−0.18, −0.04	<0.001	33,938
Topographic Wetness Index (TWI)	58	49, 67	0.95	0.07, 1.83	0.035	33,939
Spatial Null Model	65	58, 72			<0.001	33,943
Terrain Ruggedness Index (TRI)	67	59, 75	−0.12	−0.27, 0.03	0.13	33,944
Burn Severity (dNBR)	69	62, 76	−0.01	−0.02, 0.00	<0.001	33,946
Topographic Position Index (TPI)	64	57, 70	0.03	−0.03, 0.09	<0.001	33,948
Distance to Seed Source (DTS)	66	58, 74	−0.01	−0.03, 0.01	<0.001	33,950

Ecosystem Resilience Index						
Model	β_0	95% CI	β_1	95% CI	p-value	AIC
Annual Net Solar Radiation (SRAD)	151	140, 161	−0.03	−0.03, −0.02	<0.001	26,608
Distance to Seed Source (DTS)	68	64, 72	−0.07	−0.08, −0.06	<0.001	26,775
Burn Severity (dNBR)	64	59, 69	−0.02	−0.02, −0.02	<0.001	26,828
Available Soil Water Storage Capacity (AWS)	23	16, 31	0.26	0.21, 0.30	<0.001	26,866
Climate Water Deficit (CWD)	92	82, 101	−0.14	−0.17, −0.11	<0.001	26,916
Topographic Wetness Index (TWI)	45	39,51	1.24	0.86, 1.6	<0.001	26,951
Topographic Position Index (TPI)	54	48, 60	−0.08	−0.11, −0.05	<0.001	26,967
Cold Air Drainage (CAD)	42	34, 51	−4.60	−6.9, −2.3	<0.001	26,974
Spatial Null Model	54	48, 59			<0.001	26,990
Terrain Ruggedness Index (TRI)	56	51, 60	−0.08	−0.15, −0.02	0.014	26,991

4. Discussion

4.1. *Ecosystem function does not recover quickly and is primarily influenced by burn severity and topographic diversity*

Contrary to our hypothesis and many studies, ecosystem function, as measured by NPP, did not recover faster than structural and compositional metrics. Seventeen years after the wildfire, the mean functional recovery was 35 %, with an annual recovery rate of 2.0 % per year. These results align with (Yang et al. 2017), who reported minimal recovery within the first 10 years following wildfires in high latitude temperate and boreal regions. However, other studies have observed faster recovery of NDVI and GPP in boreal regions, including Alaska and Canada (Madani et al. 2021; M. O. Jones, Kimball, and Jones 2013). The differences may arise from varying methodologies, particularly the inclusion of both low and high severity fires in these studies. Our study area experienced a high severity fire, which may explain the slower recovery times.

Faster recovery times have been reported when using NDVI (Ireland and Petropoulos 2015; Sparks et al. 2018), a metric that reflects vegetation cover but does not account for potential heat stress on ecosystem functions such as photosynthesis and transpiration. In contrast, the MOD17 NPP algorithm incorporates environmental constraints like minimum temperature and vapor pressure deficit (VPD). These constraints may provide a more conservative estimate of functional recovery. Additionally, the locally validated Landsat-based NPP product at 30 m resolution likely captures finer scale insights into recovery patterns, potentially offering a more accurate timeline compared to coarser-resolution studies. Therefore, the results presented in our study may reflect a more accurate timeline of functional recovery.

As predicted, burn severity emerged as the primary driver of functional recovery, with higher recovery rates observed in areas of low burn severity ($\widehat{\beta}_{\mathrm{dNBR}}$ = -0.049). This finding aligns with other studies that report burn severity as a key factor limiting recovery (Ireland and Petropoulos 2015; Bright et al. 2019). However, burn severity's influence may diminish over time, as observed in boreal forests (Jin et al. 2012).

The Terrain Ruggedness Index (TRI) played an important role in the functional recovery of the burn area, which is characterized by complex mountainous terrain. Higher TRI values ($\widehat{\beta}_{TRI} = 0.75$) appear to facilitate functional recovery, potentially due to increased microclimatic variability and resource heterogeneity associated with more rugged terrain. Although previous studies have not directly linked TRI to postfire functional recovery, topographic features are well documented as influential factors in shaping recovery patterns (Leon, Van Leeuwen, and Casady 2012). TRI has also been associated with higher biodiversity, as more complex terrain can support diverse vegetation communities (Stojilković 2022).This biodiversity-productivity relationship (Tilman, Isbell, and Cowles 2014) may partially explain the observed role of TRI in facilitating functional recovery. Interestingly, our findings did not identify TRI as an influential factor in compositional recovery, suggesting that topographic complexity may affect ecosystem function (e.g., NPP) through mechanisms other than its direct relationship with biodiversity.

Solar radiation (SRAD) was the third most important factor influencing functional recovery. While essential for photosynthesis, excessive solar radiation ($\widehat{\beta}_{SRAD} =$ -0.025) appears to hinder recovery, likely due to its impact on soil moisture availability, particularly on equatorially facing (here, south) slopes with greater solar exposure. This finding aligns with studies showing reduced postfire NDVI recovery on slopes receiving higher solar radiation (Sever, Leach, and Bren 2012; Ireland and Petropoulos 2015). Interestingly, in boreal larch forests, increased solar radiation positively influences understory NPP recovery, including shrubs and grasses that may be more light limited (Z. Liu and Yang 2014). However, in high latitude temperate forested environments, excessive radiation may exacerbate heat stress and moisture limitations, inhibiting functional recovery.

4.2. *Ecosystem structure exhibits high recovery and is primarily driven by solar radiation and seed availability*

Contrary to our predictions, ecosystem structure, as measured by canopy height, exhibited the highest percent recovery (62 %) and rate of recovery (3.6 %/yr) among the metrics examined. This finding aligns with studies reporting rapid canopy height recovery in boreal forests, where 50 % recovery has been observed within 5–10 years postfire (Bartels et al. 2016). However, our results do not align with a recent study that found that forests of the Northern Rockies subjected to fire in the preceding 25 years experienced an overall decline in canopy height (Ilangakoon et al. 2023). The discrepancy may stem from the overestimation of vegetation under 5 m in the sentinel GEDI model or that our results align more closely with boreal forests due to the higher latitude and location of our study site.

Solar radiation emerged as the strongest predictor of structural recovery, suggesting that cooler areas that receive less direct solar radiation ($\widehat{\beta}_{SRAD} = -0.037$) see higher rates of recovery. This result supports findings from (Christopoulou et al. 2019), who reported greater recovery on north-facing slopes with lower solar radiation levels. However, our findings contrast with (Clark-Wolf, Higuera, and Davis 2022), who observed a positive relationship between seedling height and warmer, drier microclimates three years postfire in a Northern Rockies site. The differences may reflect regional climatic variation; the Canadian Rockies may favor recovery in less exposed, cooler microclimates.

Distance to seed source also strongly influenced structural recovery, with higher recovery rates observed closer to existing seed sources ($\widehat{\beta}_{DTS} = -0.11$). Our results align with studies showing greater conifer regeneration within 400 m of seed sources in the Northern Rockies and Pacific Northwest (Stevens-Rumann and Morgan 2019) and sparse recovery beyond 150 m (Kiel and Turner 2022). Interestingly, our findings indicate that structural recovery $\geqq$ 70 % was achieved within 100 m of the seed source, possibly reflecting contributions from nearby postfire resprouters, such as aspen (Andrus et al. 2021; Nigro et al. 2022), documented at our site (*Figs. S11, S12*). Future research should differentiate between postfire seed-based recovery and resprouting to better understand how proximity to reproductively mature vegetation influences the recovery of ecosystem structure following wildfire.

Moisture availability further influenced recovery, with higher available soil water storage capacity ($\widehat{\beta}_{AWS} = 0.33$) facilitating recovery, while greater climate water deficit ($\widehat{\beta}_{CWD} = -0.21$) hindered it. These findings align with research in Canadian forests, where regenerating stands were sensitive to drought (Bartels et al. 2016), and studies showing Douglas fir and ponderosa pine recovery was strongly tied to soil moisture and annual climate conditions (Kim T. Davis et al. 2019). Similarly, (Marshall et al. 2023) demonstrated that seedling canopy height in postfire planting studies was positively associated with areas of higher soil moisture. Collectively, these results highlight the critical role of moisture in driving structural recovery and suggest that revegetation efforts should prioritize areas with greater overall moisture availability to enhance postfire recovery.

4.3. *Ecosystem composition experiences high recovery and is driven by energy and available moisture*

Contrary to expectations, compositional recovery exhibited the second highest percentage recovery (60 %) among ecosystem attributes, with a recovery rate of 3.53 % per year. However, postfire composition differed from prefire conditions, with perennial forbs and grasses driving recovery and replacing the tree cover that previously dominated the area (*Fig. S6*). This shift suggests a potential ecosystem transformation toward an open forest or grassland configuration. While many studies have documented shifts in tree composition following fire (Donato, Harvey, and Turner 2016; Stevens-Rumann et al. 2018), they primarily focus on the immediate regeneration of trees. By examining the relative abundance of multiple vegetation functional types, our study captures a more nuanced picture of compositional recovery, including understory dynamics often overlooked in tree-focused analyses.

Solar radiation ($\widehat{\beta}_{SRAD} =$ -0.014) emerged as the primary predictor of compositional recovery, suggesting that higher solar radiation levels may constrain vegetation regrowth due to increased temperatures and moisture stress. Structural recovery (i.e., canopy height) showed greater sensitivity to solar radiation ($\widehat{\beta}_{SRAD} =$ -0.037), indicating that tree canopy recovery is more affected by radiation than other vegetation types. These findings align with (Vanderhoof et al. 2021), who observed faster recovery of deciduous vegetation under cooler summer temperatures across the western US. This suggests that reduced solar radiation, which leads to cooler conditions, may favor the recovery of certain species, such as aspen and larch, as observed in our study area (*Figs. S7, S8, S11, S12-14*).

Moisture availability, reflected by soil water storage capacity ($\widehat{\beta}_{AWS} = 0.21$), also played a critical role in compositional recovery, a finding reflected in structural recovery. Our findings align with a study in Yellowstone National Park, where soil moisture influenced Douglas-fir and lodgepole pine germination rates (Hoecker, Hansen, and Turner 2020). Interestingly, warmer soil temperatures were also associated with higher regeneration rates, potentially explaining the positive relationship between cold air drainage and compositional recovery ($\widehat{\beta}_{CAD} = 5.1$) in our study. Areas with less cold air drainage (i.e., warmer temperatures) showed greater recovery, suggesting that nocturnal cooling may hinder compositional recovery at this site, contrary to other research on tree establishment (Harris, Drury, and Taylor 2021). Perennial forbs and grasses, which emerged as the predominant fractional cover in 2020 (*Fig. S6*), are likely better adapted to warmer temperatures and less affected by heat stress (Stevens, Miller, and Fornwalt 2019), potentially explaining the observed relationship between warmer conditions and recovery.

Overall, our findings underscore the complexity of compositional recovery postfire, highlighting that forest ecosystems are composed of more than just trees. Focusing solely on tree regeneration risks overlooking the recovery of other critical plant functional types, such as grasses and forbs, which may play an important role in shaping postfire ecosystem trajectories.

4.4. Ecosystem resilience that integrates recovery metrics is primarily driven by solar radiation, seed availability, and burn severity

Seventeen years after the Crazy Horse Fire in the Western Canadian Rockies Ecoregion, we calculated a mean Ecosystem Resilience Index (ERI) of 54 % of estimated full recovery to the preburn condition with an annual resilience rate of 3.2 %. In this region, wildfires typically recur every 120 years. At the 17-year mark, expected resilience under this fire return interval would be 13 %, or 0.83 % annually. Our observed resilience rate exceeds this baseline, suggesting the ecosystem is not undergoing a state transition or type conversion. This finding aligns with (Clark-Wolf et al. 2023), who reported that contemporary fire return intervals in the region remain consistent with those observed in paleo-charcoal records.

Comparing resilience metrics across studies is challenging due to differing methodologies. For example, Bryant et al. (2019) developed a unitless resilience score for structural recovery in dry-mixed conifer and ponderosa pine forests, which limits direct comparison to our ERI (%/yr). However, our findings align with projections by Davis et al. (2023) that climate conditions in the Northern Rockies will support regeneration into the mid-century, particularly in cooler, wetter areas. This contrasts with the southwestern US, where increased drought and warming temperatures are predicted to reduce forest resilience (Kimberley T. Davis et al. 2023). These regional differences underscore the importance of considering local ecological and climatic factors in resilience assessments, pointing to the utility of our resilience index across different ecoregions.

Resilience at the Crazy Horse Fire domain was most influenced by solar radiation, distance to seed source, and burn severity. The Mission Wilderness offers a unique climate refugia within the traditionally dry environments of western Montana and is shaped by advected moisture from Flathead Lake, creating conditions more typical of the cooler, moister Pacific Northwest. Therefore, we would expect resilience to wildfire to be less moisture limited and more energy limited in this area. Solar radiation emerged as a key predictor of resilience, with a negative overall relationship ($\widehat{\beta}_{\text{SRAD}}$ = -0.026), suggesting that the system is not energy-limited but instead experiences vegetation stress under higher solar radiation. Sensitivities differed among ecosystem attributes: structure ($\widehat{\beta}_{\text{SRAD}} = -0.04$) and function ($\widehat{\beta}_{\text{SRAD}}$ = -0.03) were more affected than composition ($\widehat{\beta}_{\text{SRAD}}$ = -0.01).

Distance to seed source ($\widehat{\beta}_{\text{DTS}} = -0.069$) was an important predictor of resilience, yet of the ecosystem attributes, it only strongly predicted structural recovery. This suggests that while seed availability is critical for germination, it may be less relevant for seedling survival or in areas experiencing compositional shifts. Burn severity ($\widehat{\beta}_{\text{dNBR}}$ = -0.022) also emerged as a key predictor of resilience, consistent with established literature (Kimberley T. Davis et al. 2023; Stevens-Rumann and Morgan 2019). It was the primary driver of functional recovery ($\widehat{\beta}_{\text{dNBR}} = -0.05$), but had limited influence on structural and compositional recovery, underscoring the complexity of postfire ecosystem dynamics. Together these results demonstrate the complex nature of ecosystem dynamics following wildfire. Our findings highlight the importance of adopting a comprehensive approach to resilience rather than depending on a single postfire measure.

4.5. Future directions and limitations

In this study, we demonstrate proof-of-concept for a novel Ecological Resilience Index that is applied at a landscape scale, with scalability to regional and global scales. Satellite and airborne remote sensing are extremely beneficial in that they have the ability to characterize ecological changes over large spatiotemporal scales that are inaccessible to field-based methods alone. However, these technologies have inherent limitations. Processes like soil biogeochemical cycling and erosion, which require detailed field and laboratory measurements, remain difficult to capture remotely. Incorporating field validation into regional analyses would enhance accuracy, leveraging extensive postfire recovery datasets from the western US.

The global availability of recovery metrics for ecosystem attributes offers scalability that would not be possible with field measurements alone. Ecosystem function metrics, such as productivity, are operationally available at a 500 m resolution worldwide (S. Running and Zhao 2021). Similarly, coarse resolution global metrics for structure (i.e., biomass) (R. O. Dubayah et al. 2022) and ecosystem composition (e.g., vegetation classification) are available at increasingly finer scales (DiMiceli, Sohlberg, and Townshend 2022; Brown et al. 2022). These datasets allow the integration of function, structure, and composition into a unified resilience framework applicable across ecosystems and disturbances.

We reviewed available remote sensing datasets to combine data products capturing the three critical ecosystem attributes of resilience: function, structure, and composition. For ecosystem function, we used a high resolution, locally validated NPP product developed for the conterminous US, which improves upon the global MOD17 algorithm (S. W. Running et al. 2004). Despite these advancements, the algorithm remains susceptible to NDVI saturation at high levels of greenness, which can skew estimates in postfire landscapes dominated by rapidly recovering grasses and shrubs. Additionally, the algorithm does not account for changes in atmospheric CO_2 concentrations, which can influence primary productivity over decadal timescales.

In our analysis, we assumed stationarity of NPP due to the limitations of the temporally discontinuous structural recovery metric of canopy height. As a result, we could not account for baseline shifts in NPP driven by climate changes over the 34 year study period. This assumption may have led to overestimating recovery rates in areas where elevated atmospheric CO_2 enhanced productivity or underestimating them in regions affected by prolonged drought. Addressing these limitations in future analyses could improve the accuracy of resilience assessments.

We acknowledge the limitations presented by our compositional analysis, as it does not provide species level estimates of recovery. Although the vegetation change detection algorithm has been optimized for rangelands, it has the ability to detect changes in tree cover (Allred, Bestelmeyer, and Boyd 2021). It successfully captures patterns of change within the fire and can identify quantifiable changes at the pixel level. Another benefit of this analysis is that it can identify reorganization, an important aspect of resilience (Seidl and Turner 2022) and potential ecosystem transformations. Continued advancements in hyperspectral imaging highlight the potential for improved monitoring and understanding of vegetation dynamics on both local and global scales.

To identify the most important predictors of recovery and resilience in our study domain, we constructed single-variable models rather than multivariable models. Our primary goal was to rank individual variables by their predictive power rather than develop a comprehensive recovery model. Initially, we explored multivariate models, creating 2,048 permutations to account for each permutation of variables across ecosystem attributes and resilience. While multivariate models yielded larger reductions in AIC values compared to single-variable models, the differences were negligible. For instance, the top 10 multivariate models predicting functional recovery reduced AIC values by 2 points or less, and the top 26 models achieved reductions of only 4 points or less. These minimal differences made it difficult to discern the most influential predictors of recovery and resilience following wildfire. Small AIC differences may also be attributed to overlapping characteristics among environmental driver variables. For example, terrain indices such as TPI, TWI, and AWS, all represent variations in landscape moisture. These shared characteristics likely reduce the distinctiveness of individual variables in multivariate models. Future analyses over broader regions may reveal larger AIC differences in multivariate models, aiding in the development of a comprehensive predictive model for recovery and resilience.

Arguments over the true meaning of resilience are common, and criticism of our Ecosystem Resilience Index is expected. However, our novel approach does not rely on any single recovery metric, but rather incorporates several metrics quantitatively into a multi-dimensional resilience index. We present a flexible index that can be altered to include different recovery metrics and be applied to other disturbances like drought or bark beetle infestation. We look forward to people applying our ERI to other ecosystems and building upon it to include other recovery metrics, field data, or sources of error that can be incorporated into our weighting scheme.

5. Conclusion

In this study, we examined how the rate and percent of recovery varied across ecosystem function, structure, and composition attributes following wildfire and identified drivers of recovery and resilience. Seventeen years after the Crazy Horse wildfire, ecosystem structure showed the greatest recovery, followed by composition and function. Our predictions that environmental drivers varied across ecosystem attributes and the synthesized resilience index were confirmed. These results demonstrate that examining singular ecosystem attributes is insufficient to quantify ecosystem resilience.

This study unifies concepts on ecological resilience to wildfire providing a proof-of-concept that can be applied to other ecosystems and disturbances. Our work combines existing and emerging remote sensing technologies that increase our understanding of ecosystem characteristics that contribute to resilience and the biotic and abiotic mechanisms explaining their variability at the landscape scale. The Ecosystem Resilience Index is applicable to forest management and conservation to better target ecosystems and microclimates where revegetation efforts may have the greatest success following fire, or alternatively where these efforts may be unsuccessful based on physical or biological limitations. Although our work focuses on a single disturbance agent (wildfire) in a forested ecosystem, the flexible framework we developed is intended to be broadly applicable to multiple disturbance agents occurring across varying ecosystems. This research contributes to our understanding of ecosystem resilience to disturbance in general and specifically to fire as an agent of disturbance and how it might be reshaping our ecosystems.

CRediT authorship contribution statement

Marie Johnson: Writing – review & editing, Writing – original draft, Visualization, Software, Methodology, Investigation, Funding acquisition, Formal analysis, Data curation, Conceptualization. **Ashley Ballantyne:** Writing – review & editing, Supervision, Resources, Methodology, Investigation, Funding acquisition, Conceptualization. **Jon Graham:** Writing – review & editing, Software, Methodology, Formal analysis. **Zachary Holden:** Writing – review & editing, Resources, Data curation. **Zachary Hoylman:** Writing – review & editing, Resources, Data curation. **Kelsey Jensco:** Writing – review & editing, Conceptualization. **David Ketchum:** Writing – review & editing, Software, Methodology, Formal analysis. **John Kimball:** Writing – review & editing, Conceptualization. **Jessica Mitchell:** Writing – review & editing, Conceptualization.

Declaration of competing interest

The authors declare that they have no known competing financial interests or personal relationships that could have appeared to influence the work reported in this paper.

Acknowledgments

This research was supported by the National Aeronautics Space Administration FINESST program (80NSSC22K1550).

Appendix A. Supplementary data

Supplementary data to this article can be found online at https://doi.org/10.1016/j.ecolind.2025.113076.

Data availability

All data used in this research are publicly available on Google Earth Engine.

References

Abatzoglou, J.T., Park Williams, A., 2016. Impact of Anthropogenic Climate Change on Wildfire across Western US Forests. PNAS 113 (42), 11770.

Albrich, K., Rammer, W., Turner, M.G., Ratajczak, Z., Braziunas, K.H., Hansen, W.D., Seidl, R., 2020. Simulating Forest Resilience: A Review. Glob. Ecol. Biogeogr. 29 (12), 2082–2096.

Allen, C.R., Angeler, D.G., Cumming, G.S., Folke, C., Twidwell, D., Uden, D.R., 2016. Quantifying Spatial Resilience. J. Appl. Ecol. 53 (3), 625–635.

Allred, B.W., Bestelmeyer, B.T., Boyd, C.S., 2021. Improving Landsat Predictions of Rangeland Fractional Cover with Multitask Learning and Uncertainty. Methods in Ecology and Evolution / British Ecological Society.

Alt, M., McWethy, D.B., Everett, R., Whitlock, C., 2018. Millennial Scale Climate-Fire-Vegetation Interactions in a Mid-Elevation Mixed Coniferous Forest, Mission Range, Northwestern Montana, USA. Quat. Res. 90 (1), 66–82.

Andrus, R.A., Hart, S.J., Tutland, N., Veblen, T.T., 2021. Future Dominance by Quaking Aspen Expected Following Short-interval, Compounded Disturbance Interaction. Ecosphere 12 (1).

Bartels, S.F., Chen, H.Y.H., Wulder, M.A., White, J.C., 2016. Trends in Post-Disturbance Recovery Rates of Canada's Forests Following Wildfire and Harvest. For. Ecol. Manage. 361, 194–207.

J.K. Berkey R. Travis Belote C.T. Maher A.J. Larson "Structural Diversity and Development in Active Fire Regime Mixed-Conifer Forests". Forest Ecology and Management 479 2021.

Beven, K.J., Kirkby, M.J., 1979. A Physically Based, Variable Contributing Area Model of Basin Hydrology / Un Modèle à Base Physique de Zone D'appel Variable de L'hydrologie Du Bassin Versant. Hydrol. Sci. Bull. 24 (1), 43–69.

Bivand, Roger S., Edzer J. Pebesma, and Virgilio Gomez-Rubio. 2013. *Applied Spatial Data Analysis with R*. Use R! 10. New York, NY: Springer.

Bolton, D.K., Coops, N.C., Wulder, M.A., 2015. Characterizing Residual Structure and Forest Recovery Following High-Severity Fire in the Western Boreal of Canada Using Landsat Time-Series and Airborne Lidar Data. Remote Sens. Environ. 163, 48–60.

Bonan, G.B., 2008. Forests and Climate Change: Forcings, Feedbacks, and the Climate Benefits of Forests. Science 320 (5882), 1444.

Bowman, D.M.J.S., Balch, J.K., Artaxo, P., Bond, W.J., Carlson, J.M., Cochrane, M.A., D'Antonio, C.M., et al., 2009. Fire in the Earth System. Science 324 (5926), 481.

Breiman, L., 2001. Random Forests. Mach. Learn. 45 (1), 5–32.

Bright, B.C., Hudak, A.T., Kennedy, R.E., Braaten, J.D., Khalyani, A.H., 2019. Examining Post-Fire Vegetation Recovery with Landsat Time Series Analysis in Three Western North American Forest Types. Fire Ecol. 15 (1), 8.

Brown, C.F., Brumby, S.P., Guzder-Williams, B., Birch, T., Hyde, S.B., Mazzariello, J., Czerwinski, W., et al., 2022. Dynamic World, Near Real-Time Global 10 M Land Use Land Cover Mapping. Sci. Data 9 (1), 1–17.

Bryant, T., Waring, K., Meador, A.S., Bradford, J.B., 2019. A Framework for Quantifying Resilience to Forest Disturbance. Front. For. Global Change 2, 56.

Busby, S.U., Moffett, K.B., Holz, A., 2020. High-severity and Short-interval Wildfires Limit Forest Recovery in the Central Cascade Range. Ecosphere 11 (9).

Calkin, D., Hyde, K., Gebert, K., Jones, G., 2005. Comparing Resource Values at Risk from Wildfires with Forest Service Fire Suppression Expenditures: Examples from 2003 Western Montana Wildfire Season. USDA Forest Service - Research Note RMRS-RN no. 24 RMRS-RN, 1–8.

Chambers, J.C., Allen, C.R., Cushman, S.A., 2019. Operationalizing Ecological Resilience Concepts for Managing Species and Ecosystems at Risk. Frontiers in Ecology and Evolution 7.

Christopoulou, A., Mallinis, G., Vassilakis, E., Farangitakis, G.-P., Fyllas, N.M., Kokkoris, G.D., Arianoutsou, M., 2019. Assessing the Impact of Different Landscape Features on Post-Fire Forest Recovery with Multitemporal Remote Sensing Data: The Case of Mount Taygetos (southern Greece). Int. J. Wildland Fire 28 (7), 521–532.

Clark-Wolf, K., Higuera, P.E., Davis, K.T., 2022. Conifer Seedling Demography Reveals Mechanisms of Initial Forest Resilience to Wildfires in the Northern Rocky Mountains. For. Ecol. Manage. 523 (November), 120487.

Clark-Wolf, K., Higuera, P.E., Shuman, B.N., McLauchlan, K.K., 2023. Wildfire Activity in Northern Rocky Mountain Subalpine Forests Still within Millennial-Scale Range of Variability. Environ. Res.Letters: ERL [web Site] 18 (9), 094029.

Coop, J.D., Parks, S.A., Stevens-Rumann, C.S., Crausbay, S.D., Higuera, P.E., Hurteau, M. D., Tepley, A., et al., 2020. Wildfire-Driven Forest Conversion in Western North American Landscapes. Bioscience 70 (8), 659–673.

Cressie, N., Hawkins, D.M., 1980. Robust Estimation of the Variogram: I. J. Int. Assoc. Math. Geol. 12 (2), 115–125.

Davis, K.T., Dobrowski, S.Z., Higuera, P.E., Holden, Z.A., Veblen, T.T., Rother, M.T., Parks, S.A., Sala, A., Maneta, M., 2019. Wildfires and Climate Change Push Low-Elevation Forests across a Critical Climate Threshold for Tree Regeneration. *Proceedings of the National Academy of Sciences* in Press.

Davis, T.S., Meddens, A.J.H., Stevens-Rumann, C.S., Jansen, V.S., Sibold, J.S., Battaglia, M.A., 2022. Monitoring Resistance and Resilience Using Carbon Trajectories: Analysis of Forest Management-Disturbance Interactions. Ecological Applications: A Publication of the Ecological Society of America 32 (8), e2704.

Davis, K.T., Robles, M.D., Kemp, K.B., Higuera, P.E., Chapman, T., Metlen, K.L., Peeler, J. L., et al., 2023. Reduced Fire Severity Offers near-Term Buffer to Climate-Driven Declines in Conifer Resilience across the Western United States. PNAS 120 (11), e2208120120.

DiMiceli, Charlene, Robert Sohlberg, and John Townshend. 2022. "MODIS/Terra Vegetation Continuous Fields Yearly L3 Global 250m SIN Grid V061." NASA EOSDIS Land Processes Distributed Active Archive Center.

Donato, D.C., Harvey, B.J., Turner, M.G., 2016. Regeneration of Montane Forests 24 Years Afer the 1988 Yellowstone Fires: A Fire-Catalyzed Shif in Lower Treelines? Ecosphere 7 (8), 1–16.

Dubayah, R., Blair, J.B., Goetz, S., Fatoyinbo, L., Hansen, M., Healey, S., Hofton, M., et al., 2020. The Global Ecosystem Dynamics Investigation: High-Resolution Laser Ranging of the Earth's Forests and Topography. Egyptian Journal of Remote Sensing and Space Sciences 1 (June), 100002.

Dubayah, R. O., J. Armston, J. R. Kellner, L. Duncanson, S. P. Healey, P. L. Patterson, S. Hancock, et al. 2022. "GEDI L4A Footprint Level Aboveground Biomass Density, Version 2.1." ORNL DAAC.

Dumelle, M., Higham, M., Ver Hoef, J.M., 2023. Spmodel: Spatial Statistical Modeling and Prediction in R. PLoS One 18 (3), e0282524.

Eidenshink, J., Schwind, B., Brewer, K., Zhu, Z.-L., Quayle, B., Howard, S., 2007. A Project for Monitoring Trends in Burn Severity. Fire Ecol. 3 (1), 3–21.

Ferrier, S., Harwood, T.D., Ware, C., Hoskins, A.J., 2020. A Globally Applicable Indicator of the Capacity of Terrestrial Ecosystems to Retain Biological Diversity under Climate Change: The Bioclimatic Ecosystem Resilience Index. Ecol. Ind. 117 (October), 106554.

Frolking, S., Palace, M.W., Clark, D.B., Chambers, J.Q., Shugart, H.H., Hurtt, G.C., 2009. Forest Disturbance and Recovery: A General Review in the Context of Spaceborne Remote Sensing of Impacts on Aboveground Biomass and Canopy Structure. J. Geophys. Res. Biogeo. 114 (3).

Goetz, S.J., Fiske, G.J., Bunn, A.G., 2006. Using Satellite Time-Series Data Sets to Analyze Fire Disturbance and Forest Recovery across Canada. Remote Sens. Environ. 101 (3), 352–365.

Gorelick, N., Hancher, M., Dixon, M., Ilyushchenko, S., Thau, D., Moore, R., 2017. Google Earth Engine: Planetary-Scale Geospatial Analysis for Everyone. Remote Sens. Environ. 202, 18–27.

Greenberg, C.H., Collins, B.S., Goodrick, S., Stambaugh, M.C., Wein, G.R., 2021. Introduction to Fire Ecology Across USA Forested Ecosystems: Past, Present, and Future. In: Greenberg, C.H., Collins, B. (Eds.), Fire Ecology and Management: past, Present, and Future of US Forested Ecosystems. Springer International Publishing, Cham, pp. 1–30.

Gunderson, L.H., 2000. Ecological Resilience—In Theory and Application. Annu. Rev. Ecol. Syst. 31 (1), 425–439.

Hagmann, R.K., Hessburg, P.F., Prichard, S.J., Povak, N.A., Brown, P.M., Fulé, P.Z., Keane, R.E., et al., 2021. Evidence for Widespread Changes in the Structure, Composition, and Fire Regimes of Western North American Forests. Ecological Applications: A Publication of the Ecological Society of America 31 (8), e02431.

Harris, L.B., Drury, S.A., Taylor, A.H., 2021. Strong Legacy Effects of Prior Burn Severity on Forest Resilience to a High-Severity Fire. Ecosystems 24 (4), 774–787.

Hastie, T., Tibshirani, R., Friedman, J.H., 2001. The Elements of Statistical Learning: Data Mining, Inference, and Prediction. Springer Science & Business Media.

Hicke, J.A., Asner, G.P., Kasischke, E.S., French, N.H.F., Randerson, J.T., James Collatz, G., Stocks, B.J., Tucker, C.J., Los, S.O., Field, C.B., 2003. Postfire Response of North American Boreal Forest Net Primary Productivity Analyzed with Satellite Observations. Glob. Chang. Biol. 9 (8), 1145–1157.

Higuera, P.E., Shuman, B.N., Wolf, K.D., 2021. Rocky Mountain Subalpine Forests Now Burning More than Any Time in Recent Millennia. In: Proceedings of the National Academy of Sciences of the United States of America, p. 118.

Hoecker, T.J., Hansen, W.D., Turner, M.G., 2020. Topographic Position Amplifies Consequences of Short-Interval Stand-Replacing Fires on Postfire Tree Establishment in Subalpine Conifer Forests. For. Ecol. Manage. 478 (December), 118523.

Hoef, V., Jay, M., Peterson, E.E., Hooten, M.B., Hanks, E.M., Fortin, M.J., 2018. Spatial Autoregressive Models for Statistical Inference from Ecological Data. Ecol. Monogr. 88 (1), 36–59.

Holden, Z.A., Swanson, A., Luce, C.H., Matt Jolly, W., Maneta, M., Oyler, J.W., Warren, D.A., Parsons, R., Affleck, D., 2018. Decreasing Fire Season Precipitation Increased Recent Western US Forest Wildfire Activity. PNAS 115 (36), E8349.

Holden, Z.A., Warren, D., Davis, K., Jungck, E., Maneta, M., Dobrowski, S., Archer, V., 2022. REGEN MAPPER: A Web-Based Tool for Predicting Postfire Conifer Regeneration and Prioritizing Reforestation Efforts in the Western United States. Foundational Concepts in Silviculture with Emphasis on Reforestation and Early Stand Improvement - 2022 National Silviculture Workshop.

Holling, C.S., 1973. The Resilience and Stability of Ecosystems. Annual Review of Ecology and Systematics 4, 1–23.

Hoylman, Z.H., Jencso, K.G., Jia, Hu., Martin, J.T., Holden, Z.A., Seielstad, C.A., Rowell, E.M., 2018. Hillslope Topography Mediates Spatial Patterns of Ecosystem Sensitivity to Climate. J. Geophys. Res. Biogeo. 123 (2), 353–371.

Hoylman, Z.H., Jencso, K., Archer, V., Efta, J.A., 2021. The Influence of Hydroclimate and Management on Forest Regrowth across the Western US. The. Environmentalist.

Hudak, A.T., Crookston, N.L., Evans, J.S., Hall, D.E., Falkowski, M.J., 2008. Nearest Neighbor Imputation of Species-Level, Plot-Scale Forest Structure Attributes from LiDAR Data. Remote Sensing of Environment 112 (5), 2232–2245.

Hwang, K., Harpold, A.A., Tague, C.L., Lowman, L., Boisramé, G.F.S., Lininger, K.B., Sullivan, P.L., et al., 2023. "Seeing the Disturbed Forest for the Trees: Remote Sensing Is Underutilized to Quantify Critical Zone Response to Unprecedented Disturbance". *Earth's*. Future 11 (8).

Ibáñez, I., Acharya, K., Juno, E., Karounos, C., Lee, B.R., McCollum, C., Schaffer-Morrison, S., Tourville, J., 2019. Forest Resilience under Global Environmental Change: Do We Have the Information We Need? A Systematic Review. PLoS One 14 (9), e0222207.

Ilangakoon, Nayani, Jennifer K. Balch, R. Chelsea Nagy, and Virginia Iglesias. 2023. "Postfire Recovery of Western US Conifer Forests (1984-2017) Using Space-Borne Lidar Data." *bioRxiv*.

Ireland, G., Petropoulos, G.P., 2015. Exploring the Relationships between Post-Fire Vegetation Regeneration Dynamics, Topography and Burn Severity: A Case Study from the Montane Cordillera Ecozones of Western Canada. Appl. Geogr. 56, 232–248.

Jin, Y., Randerson, J.T., Goetz, S.J., Beck, P.S.A., Loranty, M.M., Goulden, M.L., 2012. The Influence of Burn Severity on Postfire Vegetation Recovery and Albedo Change during Early Succession in North American Boreal Forests. J. Geophys. Res. 117 (G1).

Jones, Matthew O., Brady W. Allred, David E. Naugle, Jeremy D. Maestas, Patrick Donnelly, Loretta J. Metz, Jason Karl, et al. 2018. "Innovation in Rangeland Monitoring: Annual, 30 M, Plant Functional Type Percent Cover Maps for U.S. Rangelands, 1984–2017." *Ecosphere* 9 (9).

Jones, M.O., Kimball, J.S., Jones, L.A., 2013. Satellite Microwave Detection of Boreal Forest Recovery from the Extreme 2004 Wildfires in Alaska and Canada. Glob. Chang. Biol.

Keane, R.E., Loehman, R.A., Holsinger, L.M., Falk, D.A., Higuera, P., Hood, S.M., Hessburg, P.F., 2018. Use of Landscape Simulation Modeling to Quantify Resilience for Ecological Applications. Ecosphere.

Keyser, A., Westerling, A.L., 2017. Climate Drives Inter-Annual Variability in Probability of High Severity Fire Occurrence in the Western United States. Environmental Research Letters: ERL [web Site] 12 (6).

Kiel, N.G., Turner, M.G., 2022. Where Are the Trees? Extent, Configuration, and Drivers of Poor Forest Recovery 30 Years after the 1988 Yellowstone Fires. For. Ecol. Manage. 524 (November), 120536.

Koontz, M.J., North, M.P., Werner, C.M., Fick, S.E., Latimer, A.M., 2019. "Local Forest Structure Variability Increases Resilience to Wildfire in Dry Western U. S. Coniferous Forests" 1–27.

Lang, N., Jetz, W., Schindler, K., Wegner, J.D., 2023. A High-Resolution Canopy Height Model of the Earth. Nat. Ecol. Evol. 7 (11), 1778–1789.

Lee, C.H., Cook, S., Lee, J.S., Han, B., 2016. Comparison of Two Meta-Analysis Methods: Inverse-Variance-Weighted Average and Weighted Sum of Z-Scores. Genomics & Informatics 14 (4), 173–180.

Leon, J.R., Romo, W.J.D., Leeuwen, V., Casady, G.M., 2012. Using MODIS-NDVI for the Modeling of Post-Wildfire Vegetation Response as a Function of Environmental Conditions and Pre-Fire Restoration Treatments. Remote Sensing 4 (3), 598–621.

Li, X., Zhang, H., Yang, G., Ding, Y., Zhao, J., 2018. Post-Fire Vegetation Succession and Surface Energy Fluxes Derived from Remote Sensing. Remote Sens. (Basel) 10 (7), 1000.

Liu, Z., Ballantyne, A.P., Annie Cooper, L., 2019. Biophysical Feedback of Global Forest Fires on Surface Temperature. Nat. Commun. 10 (1), 214.

Liu, A., Cheng, X., Chen, Z., 2021. Performance Evaluation of GEDI and ICESat-2 Laser Altimeter Data for Terrain and Canopy Height Retrievals. Remote Sens. Environ. 264 (October), 112571.

Liu, Z., Yang, J., 2014. Quantifying Ecological Drivers of Ecosystem Productivity of the Early-successional Boreal *Larix Gmelinii* Forest. Ecosphere 5 (7), 1–16.

Lydersen, J., North, M., 2012. Topographic Variation in Structure of Mixed-Conifer Forests Under an Active-Fire Regime. Ecosystems 15 (7), 1134–1146.

Mack, M.C., Treseder, K.K., Manies, K.L., Harden, J.W., Schuur, E.A.G., Vogel, J.G., Randerson, J.T., Stuart Chapin, F., 2008. Recovery of Aboveground Plant Biomass and Productivity after Fire in Mesic and Dry Black Spruce Forests of Interior Alaska. Ecosystems 11 (2), 209–225.

Madani, N., Parazoo, N.C., Kimball, J.S., Reichle, R.H., Chatterjee, A., Watts, J.D., Saatchi, S., et al., 2021. The Impacts of Climate and Wildfire on Ecosystem Gross Primary Productivity in Alaska. J. Geophys. Res. Biogeo. 126 (6).

Mansuy, N., Gauthier, S., Robitaille, A., 2012. "Regional Patterns of Postfire Canopy Recovery in the Northern Boreal Forest of Quebec: Interactions between Surficial Deposit. Climate, and Fire Cycle". *Canadian Journal of*.

Marsh, C., Crockett, J.L., Krofcheck, D., Keyser, A., Allen, C.D., Litvak, M., Hurteau, M.D., 2022. Planted Seedling Survival in a Post-Wildfire Landscape: From Experimental

Planting to Predictive Probabilistic Surfaces. For. Ecol. Manage. 525 (December), 120524.
Marshall, L.A.E., Fornwalt, P.J., Stevens-Rumann, C.S., Rodman, K.C., Rhoades, C.C., Zimlinghaus, K., Chapman, T.B., Schloegel, C.A., 2023. North-Facing Aspects, Shade Objects, and Microtopographic Depressions Promote the Survival and Growth of Tree Seedlings Planted after Wildfire. Fire Ecol. 19 (1), 26.
McIntyre, P.J., Thorne, J.H., Dolanc, C.R., Flint, A.L., Flint, L.E., Kelly, M., Ackerly, D.D., 2015. Twentieth-Century Shifts in Forest Structure in California: Denser Forests, Smaller Trees, and Increased Dominance of Oaks. Proc. Natl. Acad. Sci. 112 (5), 1458–1463.
Morford, S.L., Allred, B.W., Twidwell, D., Jones, M.O., Maestas, J.D., Naugle, D.E., 2021. "Tree Encroachment Threatens the Conservation Potential and Sustainability of U.S. Rangelands". *Biorxiv*.
Nigro, K.M., Rocca, M.E., Battaglia, M.A., Coop, J.D., Redmond, M.D., 2022. Wildfire Catalyzes Upward Range Expansion of Trembling Aspen in Southern Rocky Mountain Beetle-killed Forests. J. Biogeogr. 49 (1), 201–214.
Omernik, J.M., Griffith, G.E., 2014. Ecoregions of the Conterminous United States: Evolution of a Hierarchical Spatial Framework. Environ. Manag. 54 (6), 1249–1266.
Pan, Y., Birdsey, R.A., Fang, J., Houghton, R., Kauppi, P.E., Kurz, W.A., Phillips, O.L., et al., 2011. A Large and Persistent Carbon Sink in the World's Forests. Science 333 (6045), 988–993.
Parker, A.J., 1982. THE TOPOGRAPHIC RELATIVE MOISTURE INDEX: AN APPROACH TO SOIL-MOISTURE ASSESSMENT IN MOUNTAIN TERRAIN. Phys. Geogr. 3 (2), 160.
Prichard, S.J., Povak, N.A., Kennedy, M.C., Peterson, D.W., 2020. Fuel Treatment Effectiveness in the Context of Landform, Vegetation, and Large, Wind-Driven Wildfires. Ecological Applications: A Publication of the Ecological Society of America 30 (5), e02104.
PRISM Climate Group. 2014. "Oregon State University.".
Rabus, B., Eineder, M., Roth, A., Bamler, R., 2003. The Shuttle Radar Topography Mission—a New Class of Digital Elevation Models Acquired by Spaceborne Radar. ISPRS Journal of Photogrammetry and Remote Sensing: Official Publication of the International Society for Photogrammetry and Remote Sensing 57 (4), 241–262.
Reed, R.A., Finley, M.E., Romme, W.H., Turner, M.G., 1999. Aboveground Net Primary Production and Leaf-Area Index in Early Postfire Vegetation in Yellowstone National Park. Ecosystems 2 (1), 88–94.
Reu, D.e., Jeroen, J.B., Bats, M., Zwertvaegher, A., Gelorini, V., De Smedt, P., Chu, W., et al., 2013. Application of the Topographic Position Index to Heterogeneous Landscapes. Geomorphology 186, 39–49.
Riley, S.J., DeGloria, S.D., Elliot, R., 1999. Index That Quantifies Topographic Heterogeneity. Intermountain Journal of Sciences: IJS 5 (1–4), 23–27.
Robinson, N.P., Allred, B.W., Smith, W.K., Jones, M.O., Moreno, A., Erickson, T.A., Naugle, D.E., Running, S.W., 2018. Terrestrial Primary Production for the Conterminous United States Derived from Landsat 30 M and MODIS 250 M. Remote Sens. Ecol. Conserv. 4 (3), 264–280.
Running, Steve, and Maosheng Zhao. 2021. "MODIS/Terra Net Primary Production Gap-Filled Yearly L4 Global 500 M SIN Grid V061." NASA EOSDIS Land Processes Distributed Active Archive Center.
Running, S.W., Nemani, R.R., Heinsch, F.A., Zhao, M., Reeves, M., Hashimoto, H., 2004. A Continuous Satellite-Derived Measure of Global Terrestrial Primary Production. Bioscience 54 (6), 547–560.
Sakamoto, Yosiyuki, and Hirotugu Akaike. 1998. "Analysis of Cross Classified Data by AIC." In *Selected Papers of Hirotugu Akaike*, edited by Emanuel Parzen, Kunio Tanabe, and Genshiro Kitagawa, 255–67. New York, NY: Springer New York.
Scheffer, M., Carpenter, S., Foley, J.A., Folke, C., Walker, B., 2001. Catastrophic Shifts in Ecosystems. Nature 413 (6856), 591.
Seidl, R., Turner, M.G., 2022. Post-Disturbance Reorganization of Forest Ecosystems in a Changing World. Proc. Natl. Acad. Sci. 119 (28), e2202190119.
Sever, L., Leach, J., Bren, L., 2012. Remote Sensing of Post-Fire Vegetation Recovery; a Study Using Landsat 5 TM Imagery and NDVI in North-East Victoria. J. Spat. Sci. 57 (2), 175–191.
Sparks, A.M., Kolden, C.A., Smith, A.M.S., Boschetti, L., Johnson, D.M., Cochrane, M.A., 2018. Fire Intensity Impacts on Post-Fire Temperate Coniferous Forest Net Primary Productivity. Biogeosciences 15 (4), 1173–1183.
Spasojevic, M.J., Bahlai, C.A., Bradley, B.A., Butterfield, B.J., Tuanmu, M.N., Sistla, S., Wiederholt, R., Suding, K.N., 2016. Scaling up the Diversity-Resilience Relationship with Trait Databases and Remote Sensing Data: The Recovery of Productivity after Wildfire. Glob. Chang. Biol. 22 (4), 1421–1432.
Standish, R.J., Hobbs, R.J., Mayfield, M.M., Bestelmeyer, B.T., Suding, K.N., Battaglia, L. L., Eviner, V., et al., 2014. Resilience in Ecology: Abstraction, Distraction, or Where the Action Is? Biol. Conserv. 177, 43–51.
Stevens, J.T., Miller, J.E.D., Fornwalt, P.J., 2019. Fire Severity and Changing Composition of Forest Understory Plant Communities. Journal of Vegetation Science: Official Organ of the International Association for Vegetation Science 30 (6), 1099–1109.
Stevens-Rumann, C.S., Kemp, K.B., Higuera, P.E., Harvey, B.J., Rother, M.T., Donato, D. C., Morgan, P., Veblen, T.T., 2018. Evidence for Declining Forest Resilience to Wildfires under Climate Change. Blackwell Publishing Ltd, Ecology Letters.
Stevens-Rumann, C.S., Morgan, P., 2019. Tree Regeneration Following Wildfires in the Western US: A Review. Fire Ecol. 15 (1), 1–17.
Stojilković, B., 2022. Towards Transferable Use of Terrain Ruggedness Component in the Geodiversity Index. Resources 11 (2), 22.
Thompson, I., Mackey, B., McNulty, S., Mosseler, A., 2009. Forest Resilience, Biodiversity, and Climate. Change 43.
Tilman, D., Isbell, F., Cowles, J.M., 2014. Biodiversity and Ecosystem Functioning. Annu. Rev. Ecol. Evol. Syst. 45 (1), 471–493.
Turner, M.G., Tinker, D.B., Romme, W.H., Kashian, D.M., Litton, C.M., 2004. Landscape Patterns of Sapling Density, Leaf Area, and Aboveground Net Primary Production in Postfire Lodgepole Pine Forests, Yellowstone National Park (USA). Ecosystems 7 (7), 751–775.
Vanderhoof, M.K., Hawbaker, T.J., Andrea, Ku., Merriam, K., Berryman, E., Cattau, M., 2021. Tracking Rates of Postfire Conifer Regeneration vs. Deciduous Vegetation Recovery across the Western United States. Ecol. Appl.: A Publication of the Ecological Society of America 31 (2), e02237.
Walker, B.H., 2020. Resilience: What It Is and Is Not. Ecol. Soc. 25 (2).
Walker, J.J., Soulard, C.E., 2019. Phenology Patterns Indicate Recovery Trajectories of Ponderosa Pine Forests After High-Severity Fires. Remote Sens. (Basel) 11 (23), 2782.
Ward, D.S., Kloster, S., Mahowald, N.M., Rogers, B.M., Randerson, J.T., Hess, P.G., 2012. The Changing Radiative Forcing of Fires: Global Model Estimates for Past, Present and Future. Atmos. Chem. Phys. 12 (22), 10857–10886.
Wolf, K.D., Higuera, P.E., Davis, K.T., Dobrowski, S.Z., 2021. Wildfire Impacts on Forest Microclimate Vary with Biophysical Context. Ecosphere 12 (5).
Yang, J., Pan, S., Dangal, S., Zhang, B., Wang, S., Tian, H., 2017. Continental-Scale Quantification of Post-Fire Vegetation Greenness Recovery in Temperate and Boreal North America. Remote Sens. Environ. 199 (September), 277–290.